THE JOURNAL OF PHYSICAL CHEMISTRY C

Article

pubs.acs.org/JPCC

Geometry of α-Cr_2O_3(0001) as a Function of H_2O Partial Pressure

M. H. M. Ahmed,[†] X. Torrelles,[‡] J.P.W. Treacy,[†] H. Hussain,[§] C. Nicklin,[∥] P. L. Wincott,[⊥,#] D. J. Vaughan,[⊥] G. Thornton,[§] and R. Lindsay*[,†]

[†]Corrosion and Protection Centre, School of Materials, The University of Manchester, Sackville Street, Manchester, M13 9PL, U.K.

[‡]Institut de Ciència de Materials de Barcelona (CSIC), Campus UAB, 08193 Bellaterra, Spain

[§]London Centre for Nanotechnology and Department of Chemistry, University College London, 20 Gordon Street, London WC1H 0AJ, U.K.

[∥]Diamond Light Source, Harwell Science and Innovation Campus, Didcot, Oxfordshire, OX11 0DE, U.K.

[⊥]Williamson Research Centre for Molecular Environmental Science and School of Earth, Atmospheric and Environmental Sciences, The University of Manchester, M13 9PL, Manchester, U.K.

Supporting Information

ABSTRACT: Surface X-ray diffraction has been employed to elucidate the surface structure of α-Cr_2O_3(0001) as a function of water partial pressure at room temperature. In ultra high vacuum, following exposure to ~2000 Langmuir of H_2O, the surface is found to be terminated by a partially occupied double layer of chromium atoms. No evidence of adsorbed OH/H_2O is found, which is likely due to either adsorption at minority sites, or X-ray induced desorption. At a water partial pressure of ~30 mbar, a single OH/H_2O species is found to be bound atop each surface Cr atom. This adsorption geometry does not agree with that predicted by *ab initio* calculations, which may be a result of some differences between the experimental conditions and those modeled.

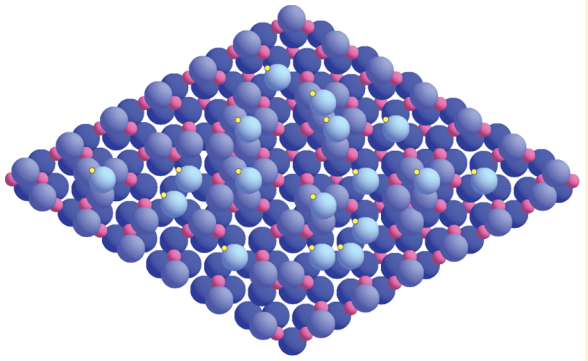

INTRODUCTION

The presence of a passive surface film is key to the exceptional corrosion resistance of stainless steel alloys.[1,2] Consequently, much effort has targeted the characterization and enhancement of this protective layer, which is often composed, at least partially, of chromia.[1,2] Such work includes fundamental studies of single crystal surfaces of α-Cr_2O_3 to gain atomic scale insight into pertinent properties, e.g., refs 3−10. To date, however, most of these measurements have been conducted in ultra high vacuum (UHV), limiting their relevance with regard to mechanistic understanding of corrosion performance in engineering environments. Targeting this omission, the current study is concerned with determining the surface structure of α-Cr_2O_3(0001) in the presence of H_2O vapor through acquisition of surface X-ray diffraction (SXRD) data; water is an essential ingredient for many corrosion phenomena.

The structure of α-Cr_2O_3(0001) as a function of both H_2O partial pressure and temperature has previously been explored by Costa et al. through *ab initio* modeling.[6] As a starting point for these calculations, a clean surface terminated by a single layer of 3-fold coordinated chromium atoms was assumed, as depicted in Figure 1A; this surface termination is labeled Cr−O_3−Cr− on the basis of its first three atomic layers (the subscript indicates the average number of atoms in each 1 × 1 unit cell). Near room temperature, it was concluded that two other terminations become energetically favorable in the presence of H_2O. At lower H_2O partial pressures, dissociative adsorption was proposed to be the most likely scenario with each surface Cr becoming decorated with two hydroxyls (OH), i.e. $(OH)_2$−Cr−O_3−; a (OH)−Cr−O_3− termination was found to be energetically unfavorable. Increasing the H_2O partial pressure resulted in the attachment of an intact H_2O molecule to each dihyroxylated Cr to form a new surface termination, i.e. $(H_2O(OH)_2)$−Cr−O_3−.

Parts B and C of Figure 1 illustrate the $(OH)_2$−Cr−O_3− and $(H_2O(OH)_2)$−Cr−O_3− adsorbate phases predicted in ref 6, including the location of the acidic hydrogen resulting from dissociative adsorption of H_2O. This moiety is bound to the topmost substrate oxygen atoms, forming a second distinct OH species. Hydrogen bonds formed between surface adsorbates (OH and H_2O) are also indicated in Figure 1, parts B and C. These theoretical structures are consistent with experimental characterization performed under UHV conditions of thin films of α-Cr_2O_3(0001) exposed to H_2O, in that at room temperature, dissociative adsorption is evident.[3,4] Moreover, the existence of two distinct OH species, as well as interadsorbate hydrogen bonding, is apparent from vibrational data.[3]

Received: May 13, 2015
Revised: August 14, 2015
Published: August 24, 2015

DOI: 10.1021/acs.jpcc.5b04607
J. Phys. Chem. C 2015, 119, 21426−21433

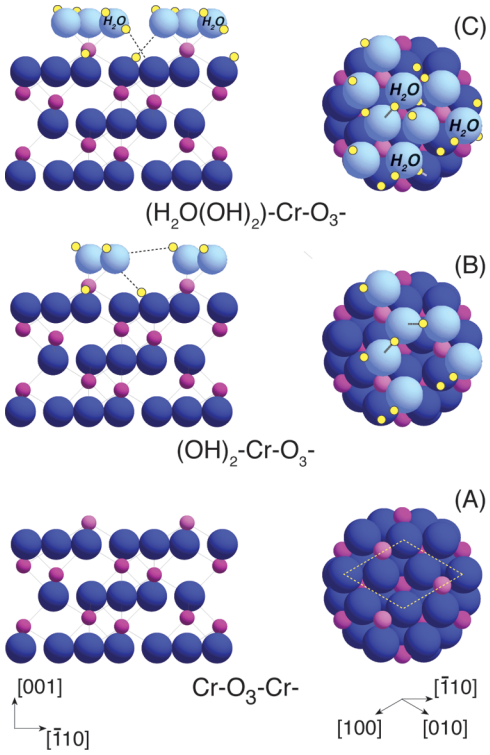

Figure 1. (A) Schematic illustration of the clean α-Cr_2O_3(0001)(1 × 1) surface employed by Costa et al. in their *ab initio* calculations of the interaction of H_2O with this substrate.[6] To the left (right) is a side (plan) view. The larger (smaller) spheres are oxygen (chromium) atoms. (B) and (C) Similar models of stable OH/H_2O decorated terminations predicted by Costa et al. at lower (B) and higher (C) H_2O partial pressures. Hydrogen bonding is indicated by means of dashed lines; the smallest spheres are hydrogen atoms. The 1 × 1 surface unit cell is indicated in the plan view in part A.

Here, the validity of the theoretical study of Costa et al.[6] is explored experimentally. Analysis of SXRD data acquired at a H_2O partial pressure of ∼30 mbar indicates that the α-Cr_2O_3(0001) surface is decorated by OH, but not exactly as predicted. This work builds on a previous SXRD study examining the impact of O_2 on the surface structure of α-Cr_2O_3(0001).[7]

EXPERIMENTAL METHODS

Experimental work was carried out at the Diamond Light Source (DLS) synchrotron facility, employing the Surface Village's off-line UHV chamber for sample preparation, and beamline I07 for SXRD measurements. *In situ* cleaning of the single crystal α-Cr_2O_3(0001) sample (supplied by PI-KEM Ltd.) involved repeated cycles of Ar^+ bombardment and annealing in UHV to approximately 1200 K. Low energy electron diffraction (LEED), and auger electron spectroscopy (AES) facilities were employed for sample characterization; LEED and AES data can be found in Supporting Information. It should be noted that following acquisition of LEED and AES data, the sample underwent a further cycle of Ar^+ bombardment and annealing to minimize the possibility of surface damage due to electron beam impingement.

Following completion of surface preparation, the sample was exposed to ∼1000 L (Langmuir) of H_2O vapor. Prior to dosing, the H_2O had been degassed through repeated freeze−pump-thaw cycles. The sample was then transferred under vacuum to I07's diffractometer in *EH1*, using a custom-built vacuum-suitcase and UHV *baby* chamber combination. The latter (base pressure ∼1 × 10^{-9} mbar) incorporates a dome shaped X-ray transparent beryllium window suitable for undertaking SXRD measurements. Once located on the beamline the sample was exposed to a further ∼1000 L of H_2O vapor; henceforth this surface will be referred to as Cr_2O_3−H_2O_{UHV}. The purpose of dosing H_2O prior to commencing diffraction measurements was to mitigate the risk of any surface contamination during the sample transfer process.

SXRD data were collected at an incidence angle of 1° with the substrate at room temperature, using a photon energy of hv =17.7 keV and a 2D Pilatus photon detector. Initially, a systematic series of X-ray reflections was acquired from Cr_2O_3−H_2O_{UHV}. More specifically, for a given *(h,k)*-integer, data were measured as a function of *l* to facilitate generation of so-called crystal truncation rods (CTRs); fractional-order rods (FORs) were also surveyed. *h, k,* and *l* are the reciprocal lattice vectors, and are defined with reference to the real space (1 × 1) unit cell of the α-Cr_2O_3(0001) surface, described by lattice vectors ($\mathbf{a_1}$, $\mathbf{a_2}$, $\mathbf{a_3}$) which are parallel to the [100], [010], [001] directions, respectively. The magnitudes of these lattice vectors are $a_1 = a_2 = a = 4.957$ Å, and $a_3 = c = 13.592$ Å,[7] where *a* and *c* are the bulk lattice constants.

Subsequent to compiling surface diffraction data from Cr_2O_3−H_2O_{UHV} in UHV, the H_2O partial pressure was increased in a stepwise fashion by appropriate backfilling of the *baby* chamber with H_2O. We note that above 1 × 10^{-4} mbar a static volume of H_2O was employed rather than obtaining an equilibrium pressure through balancing the rates of H_2O inflow and pumping, i.e. the *baby* chamber was no longer continuously pumped. For each H_2O partial pressure, the intensity of the (1, 0, 2.9) reflection was monitored to identify changes in the α-Cr_2O_3(0001) surface structure. Selection of this reflection was based upon its sensitivity to such variation as a function of O_2 partial pressure.[7] On the basis of these measurements (see below), a further systematic series of X-ray reflections was acquired from α-Cr_2O_3(0001) at a H_2O partial pressure of ∼30 mbar; henceforth this surface will be referred to as Cr_2O_3−H_2O_{30mbar}. It should be noted that as 30 mbar of H_2O is equivalent to ∼100% relative humidity with the substrate at room temperature, one would expect the surface to be submerged beneath multiple monolayers of H_2O in this environment.[11]

To facilitate fully quantitative structure determination, the raw diffraction data acquired at UHV and p(H_2O) ∼ 30 mbar were integrated and corrected[12] to enable plots of structure factor versus perpendicular momentum transfer for each CTR to be compiled. This procedure resulted in a total of 1054 (1142) nonequivalent reflections from six CTRs for Cr_2O_3−H_2O_{UHV} (Cr_2O_3−H_2O_{30mbar}). Concerning FORs, no evidence for any surface unit cell other than 1 × 1 was found.

For surface structure determination, we adopted the usual approach of generating simulated SXRD data for a series of potential model structures, and iteratively refining structural (and nonstructural) parameters to find the overall best fit between experiment and theory. The ROD software was employed for this purpose.[13] Reduced χ^2 was used to evaluate the goodness of the fit; this is defined as follows:

$$\chi^2 = \frac{1}{N-P}\sum_{i=1}^{N}\left(\frac{|F_i^{exp}(hkl)| - |F_i^{th}(hkl)|}{\sigma_i^{exp}(hkl)}\right)^2$$

DOI: 10.1021/acs.jpcc.5b04607
J. Phys. Chem. C 2015, 119, 21426−21433

N is the number of measured structure factors, P the number of parameters optimized during fitting, and $F_i^{exp}(hkl)$ and $F_i^{th}(hkl)$ are the experimental and theoretically calculated structure factors, respectively. $\sigma_i^{exp}(hkl)$ is the uncertainty associated with $F_i^{exp}(hkl)$. χ^2 behaves such that a value of 1 indicates that experiment and theory are essentially coincident, with agreement decreasing with increasing χ^2. Values of χ^2 significantly less than 1 suggest that the magnitudes of experimental uncertainties have been overestimated. The quoted precision of each fitted parameter is determined by systematically varying the parameter about its optimal value, and for each step optimizing all other parameters, until χ^2 has increased by $1/(N-P)$ from its minimum value.[14]

RESULTS

Figure 2 displays the intensity of the (1, 0, 2.9) reflection as a function of increasing H_2O partial pressure; please note, as

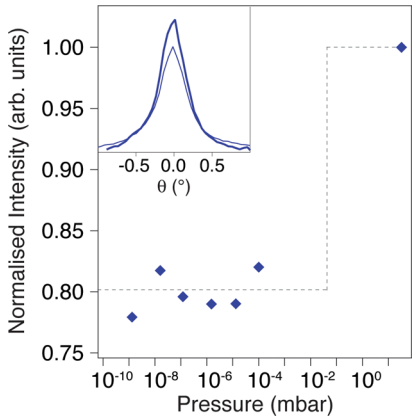

Figure 2. Plot of the intensity of the (1, 0, 2.9) reflection as a function of H_2O partial pressure; the α-Cr_2O_3(0001) sample had been dosed with ~2000 L of H_2O prior to acquisition of these data. Dashed line is a guide for the eye. Inset displays (1, 0, 2.9) rocking scans acquired at UHV (thin line) and ~30 mbar of H_2O (bold line).

described above, the sample had already been dosed with ~2000 L of H_2O prior to acquisition of these data. Upon exposure of the sample to ~30 mbar of H_2O vapor, there is an increase of ~20% in the signal. This increase is fully reversible (i.e., there is an ~20% decrease in intensity upon reducing the pressure down to $\sim 8 \times 10^{-7}$ mbar), which indicates that the change occurring at 30 mbar of H_2O is not maintained at lower vapor pressures. The inset in Figure 2 compares rocking scans acquired in UHV ($\sim 1 \times 10^{-9}$ mbar) and ~30 mbar, demonstrating the significance of the variation in reflection intensity. Furthermore, this comparison shows that there is no appreciable variation in the width of the reflection, indicating that terrace size is not significantly influenced by the presence of H_2O. These data suggest that the presence of ~30 mbar of H_2O vapor leads to a modification of the surface structure of α-Cr_2O_3(0001). This supposition will be confirmed below, through analysis of the CTR data sets acquired from Cr_2O_3–H_2O_{UHV} and Cr_2O_3–H_2O_{30mbar}.

Initially, attention was focused upon the diffraction data acquired from Cr_2O_3–H_2O_{UHV}. To begin the search for a structural solution, the clean surface structure (Cr_2O_3–$clean_{UHV}$) determined in recent quantitative LEED (LEED-IV)[15] and SXRD[7] studies was employed as a starting point. This surface exhibits a topmost partially occupied double layer of Cr atoms ($Cr_{0.31}$–$Cr_{0.61}$–$O_{2.4}$– from LEED-IV,[15] and $Cr_{0.22}$–$Cr_{0.31}$–O_3– from SXRD[7]). Given that the current measurements were undertaken following exposure to ~2000 L of H_2O, terminations with surface Cr atoms bonded to one or more OH/H_2O species were tested. It should be noted that H atoms were not explicitly included during generation of simulated of SXRD data, due to their negligible X-ray scattering, i.e. only an oxygen atom was added for each OH/H_2O. Refinement of these OH/H_2O decorated structures, including atomic coordinates, site occupation, and a surface roughness parameter (β), resulted in χ^2 values of 1.7, 2.1, and 1.8 for Cr atoms bound to one, two, or three OH/H_2O species, respectively. For completeness, a similar structural refinement was undertaken without any adsorbed OH/H_2O. Optimization of this structure resulted in a χ^2 of 1.2, indicating that the SXRD data provide no substantive evidence for adsorbed OH/H_2O under the prevailing experimental conditions.

Figure 3 displays a comparison of the experimental CTRs acquired from Cr_2O_3–H_2O_{UHV} with the best-fit theoretical simulations. To achieve this fit 41 parameters were optimized, i.e. 35 atomic coordinates, a scale factor, a surface roughness

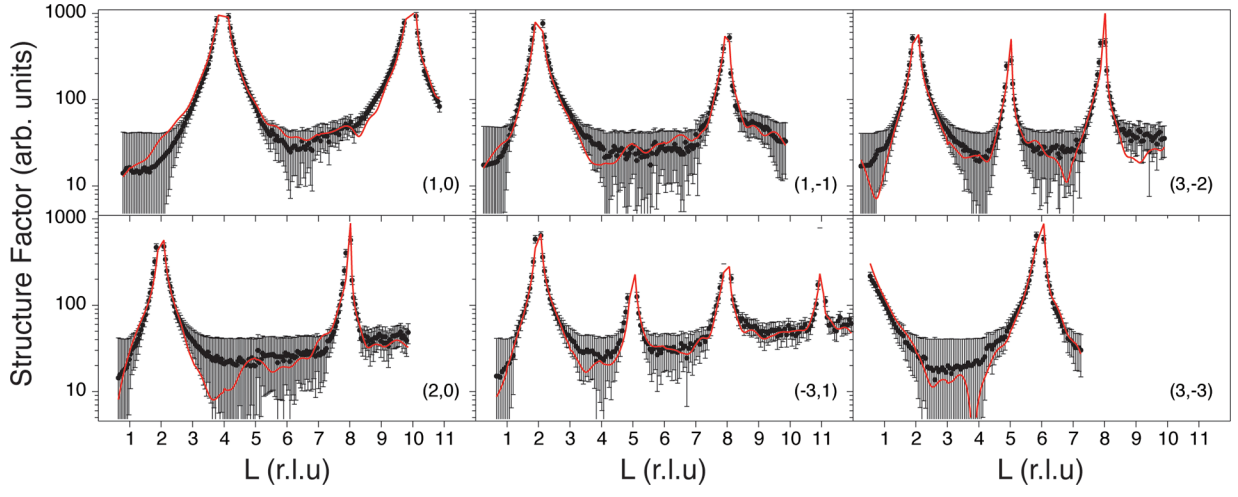

Figure 3. Comparison of experimental CTR data (solid markers with error bars), acquired from α-Cr_2O_3(0001) in UHV subsequent to exposure to ~2000 L of H_2O (Cr_2O_3–H_2O_{UHV}), and theoretical best-fit simulations (solid red lines).

DOI: 10.1021/acs.jpcc.5b04607
J. Phys. Chem. C 2015, 119, 21426–21433

parameter, and fractional occupancy factors for Cr(1), Cr(2), O(1), and Cr(3) (these atoms are identified in Figure 4);

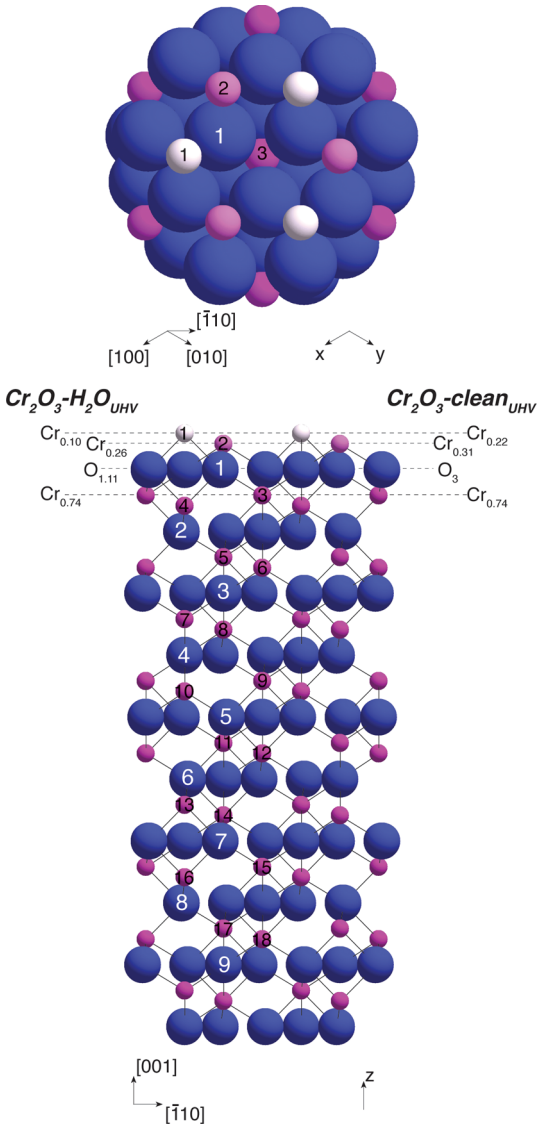

Figure 4. Schematic models of the α-$Cr_2O_3(0001)$ surface structure determined from SXRD data acquired in UHV, following exposure to ~2000 L of H_2O (Cr_2O_3–H_2O_{UHV}). At the bottom (top) is a side (plan) view. Larger (smaller) spheres are oxygen (chromium) atoms. Numerical labeling of atoms is employed for identification purposes. Layer occupancies determined for Cr_2O_3–H_2O_{UHV} (current study) and Cr_2O_3–$clean_{UHV}$[7] are indicated.

Debye–Waller factors for all atoms were maintained at bulk values, i.e., 0.5 Å^2. As may be expected for a χ^2 value of 1.2, there is a good level of agreement between theory and experiment. In a number of regions away from Bragg peaks, however, the uncertainty in the experimental structure factor is relatively large and can encompass zero. Given this situation, which may lead one to question the reliability of the optimum structure, a further structure refinement was undertaken excluding all data points where the error in the structure factor includes zero. Employing this more limited data set did not result in any significant changes in the structural solution, and so was not considered further.

The surface geometry emerging from analysis of the data acquired from Cr_2O_3–H_2O_{UHV} is illustrated in Figure 4. Corresponding atomic coordinates are listed in Table 1; all

Table 1. Optimized (x, y, z) Coordinates of Atoms Comprising the Cr_2O_3–H_2O_{UHV} Surface Derived from Analysis of the SXRD Data Presented in Figure 3[a]

	(x, y, z) coordinates (Å)	
atom	bulk-terminated	optimized
$Cr_{0.10\pm0.02}(1)$	3.31, 1.65, 22.65	*3.31**, *1.65**, 23.08 ± 0.09
$Cr_{0.26\pm0.02}(2)$	0.00, 0.00, 22.27	*0.00**, *0.00**, 22.81 ± 0.03
$O_{0.37\pm0.04}(1)$	1.79, 1.65, 21.33	1.90 ± 0.04, 1.57 ± 0.05, 21.54 ± 0.05
$Cr_{0.74\pm0.01}(3)$	1.65, 3.31, 20.39	*1.65**, *3.31**, 20.55 ± 0.01
Cr(4)	3.31, 1.65, 20.00	*3.31**, *1.65**, 19.99 ± 0.01
O(2)	1.65, −0.14, 19.06	1.68 ± 0.02, −0.14 ± 0.04, 18.89 ± 0.03
Cr(5)	0.00, 0.00, 18.12	*0.00**, *0.00**, 18.22 ± 0.01
Cr(6)	1.65, 3.31, 17.74	*1.65**, *3.31**, 17.86 ± 0.01
O(3)	1.52, 1.52, 16.80	1.53 ± 0.03, 1.56 ± 0.02, 16.90 ± 0.03
Cr(7)	3.31, 1.65, 15.86	*3.31**, *1.65**, 15.96 ± 0.01
Cr(8)	0.00, 0.00, 15.47	*0.00**, *0.00**, 15.56 ± 0.01
O(4)	1.79, 0.14, 14.53	1.80 ± 0.03, 0.05 ± 0.02, 14.60 ± 0.03
Cr(9)	1.65, 3.31, 13.59	*1.65**, *3.31**, 13.64 ± 0.01
Cr(10)	3.31, 1.65, 13.21	*3.31**, *1.65**, 13.26 ± 0.01
O(5)	1.65, 1.79, 12.27	1.62 ± 0.02, 1.74 ± 0.03, 12.17 ± 0.04
Cr(11)	0.00, 0.00, 11.33	*0.00**, *0.00**, 11.38 ± 0.01
Cr(12)	1.65, 3.31, 10.94	*1.65**, *3.31**, 10.97 ± 0.01
O(6)	1.52, 0.00, 10.00	*1.52**, *0.00**, 10.08 ± 0.03
Cr(13)	3.31, 1.65, 9.06	*3.31**, *1.65**, 9.10 ± 0.01
Cr(14)	0.00, 0.00, 8.68	*0.00**, *0.00**, 8.81 ± 0.01
O(7)	1.79, 1.65, 7.74	1.79*, 1.65*, 7.74 ± 0.02
Cr(15)	1.65, 3.31, 6.80	*1.65**, *3.31**, 6.83 ± 0.01
Cr(16)	3.31, 1.65, 6.41	*13.31**, *1.65**, 6.42 ± 0.01
O(8)	1.65, −0.14, 5.47	1.65*, −0.14*, 5.47 ± 0.02
Cr(17)	0.00, 0.00, 4.53	*0.00**, *0.00**, 4.55 ± 0.01
Cr(18)	1.65, 3.31, 4.15	*1.65**, *3.31**, 4.16 ± 0.01
O(9)	1.52, 1.52, 3.20	1.52*, 1.52*, 3.24 ± 0.03

[a]Fractional occupancy is indicated by a non-integer subscript in the "atom" column; the overall occupancy of oxygen atoms in the layer containing O(1) is 1.11 ± 0.12, as there are three symmetry equivalent oxygen atoms per (1 × 1) unit cell. Atomic coordinates for the bulk-terminated Cr–Cr–O_3-structure are also listed. Figure 4 provides a key to the identity of the atoms, and the axes x, y, and z. An asterisk (*) indicates that the parameter has been held constant during optimization. x and y coordinates not optimized due to symmetry constraints are italicized.

nearest neighbor Cr–O interatomic distances are physically reasonable. A topmost partially occupied Cr double layer is maintained in the optimized structure, although the fractional occupancies of both Cr sites are less than those determined previously for Cr_2O_3-$clean_{UHV}$;[7,15] layer occupancies determined from analysis of SXRD data from Cr_2O_3–H_2O_{UHV} (the present study) and Cr_2O_3-$clean_{UHV}$[7] are indicated in Figure 4. Atomic layer spacings perpendicular to the α-$Cr_2O_3(0001)$ surface derived from both the present results and the earlier measurements[7,15] are listed in Table 2. As with the fractional occupancies, there are variations in these values, which are not negligible. As mentioned in ref 7, a plausible explanation for these discrepancies in surface structure is that they arise from small variations in sample preparation methods, e.g. anneal temperature. Furthermore, it should be remembered that the latest SXRD data were recorded after exposure to 2000 L of

DOI: 10.1021/acs.jpcc.5b04607
J. Phys. Chem. C 2015, 119, 21426–21433

Table 2. Comparison of Atomic Layer Spacings (d_z) Perpendicular to the α-Cr_2O_3(0001) Surface Derived from Previous UHV LEED-IV[14] and SXRD[7] Work and the Current UHV SXRD Measurements Acquired Following Exposure to ~2000 L of H_2O[a]

	d_z (Å)			
atomic layers	bulk-terminated	LEED-IV, ref 14	SXRD, ref 7	SXRD, this study
Cr(1)/Cr(2)	0.38	0.27	0.22 ± 0.04	0.27 ± 0.05
Cr(2)/O(1)	0.94	1.04	1.30 ± 0.03	1.27 ± 0.05
O(1)/Cr(3)	0.94	0.96	0.68 ± 0.03	0.99 ± 0.05
Cr(3)/Cr(4)	0.38	0.38	0.33 ± 0.01	0.56 ± 0.02
Cr(4)/O(2)	0.94	0.93	0.64 ± 0.01	1.10 ± 0.02
O(2)/Cr(5)	0.94	not optimized	1.36 ± 0.01	0.67 ± 0.02

[a]Bulk terminated interlayer distances are also listed. Figure 4 indicates the identity of the atomic layers.

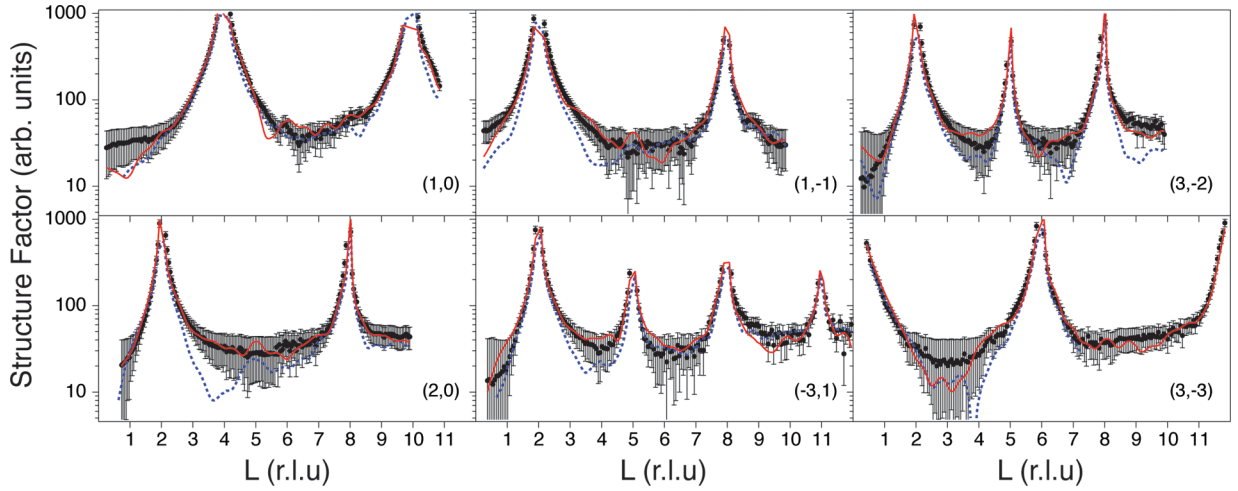

Figure 5. Comparison of experimental CTR data (solid markers with error bars), acquired from α-Cr_2O_3(0001) at p(H_2O) ~ 30 mbar (Cr_2O_3–H_2O_{30mbar}), and theoretical best-fit simulations (solid red lines). Also included are theoretically simulated data (broken blue line) for optimum Cr_2O_3–H_2O_{UHV} geometry.

H_2O, which may have induced surface modification, even though no clear evidence of surface bound OH/H_2O was found during analysis of the diffraction data. For example, a proportion of topmost oxygen atoms may in reality be OH's due to reaction with the acidic hydrogen resulting from dissociative adsorption of H_2O. The optimum value of the surface roughness parameter (β = 0.42), along with lower fractional occupancies of surface layers, may also reflect surface modification induced by H_2O exposure; β = 0.2 was obtained during fitting of the SXRD data acquired from Cr_2O_3–$clean_{UHV}$ in ref.[7] Greater surface roughness following H_2O exposure is apparently consistent with STM images acquired from a thin film of α-Cr_2O_3(0001),[4] which suggest that H_2O induces geometric disordering within terraces.

Turning to Cr_2O_3–H_2O_{30mbar}, structure determination commenced with refinement of the coordinates of the optimized Cr_2O_3–H_2O_{UHV} structure. A best-fit χ^2 of 3.2 was obtained, suggesting that the presence of ~30 mbar H_2O results in surface modification beyond mere relaxation. Consequently, terminations of the optimum Cr_2O_3–H_2O_{UHV} structure, where surface Cr atoms are bound to one or more OH/H_2O species, were tested. Refinement of these OH/H_2O decorated structures, resulted in χ^2 values of 1.1, 2.1, and 2.3 for Cr atoms bound to one, two, or three OH/H_2O species, respectively, i.e., a structure where each surface Cr is bound to a single OH/H_2O species is favored. More specifically, it is concluded that OH/H_2O is adsorbed atop Cr, at a distance of 2.09 Å; off atop adsorption was also tested, but found to increase χ^2. A comparison of the experimental CTRs with the best-fit theoretical simulations is shown in Figure 5.

Figure 6 depicts the surface structural model employed to obtain the best-fit displayed in Figure 5, in which the oxygen atoms of adsorbed OH/H_2O species are labeled with 1′, 2′, 3′, and 4′. As illustrated, the best fit was obtained with OH/H_2O (O(1′) – O(4′)) located atop Cr(1) and Cr(2), as well as above any Cr(3) and Cr(4) atoms available for bonding due to fractional occupation of the topmost oxygen layer (O(1)). It should be borne in mind that the presence of O(3′) and O(4′) does not result in unphysical interatomic distances, as the fractional occupancy of these atoms is governed by fractional occupancy of O(1). Optimum atomic coordinates are listed in Table 3. Here, again, all nearest neighbor Cr–O interatomic distances are physically reasonable. During fitting 35 atomic coordinates were varied. In addition, as above, a scale factor, a surface roughness parameter, and fractional occupancy factors for Cr(1), Cr(2), O(1), and Cr(3) were also optimized. Debye–Waller factors for all atoms were again maintained at bulk values, i.e. 0.5 $Å^2$. The optimum surface roughness parameter, β = 0.39, is very similar to that obtained for Cr_2O_3–H_2O_{UHV}, indicating that immersion in $p(H_2O)$ ~ 30 mbar does not induce further surface roughening. Furthermore, it should be noted that O(1′) and O(2′) were constrained to have the same fractional occupancies as Cr(1) and Cr(2), respectively. Similarly, the fractional occupations of O(3′) and O(4′) were fixed to be equal to the fraction of available Cr(3) and Cr(4) atoms, respectively. Finally, all Cr–OH/H_2O bond lengths (i.e., Cr(1)–O(1′), Cr(2)–O(2′), Cr(3)–O(3′), and Cr(4)–

DOI: 10.1021/acs.jpcc.5b04607
J. Phys. Chem. C 2015, 119, 21426–21433

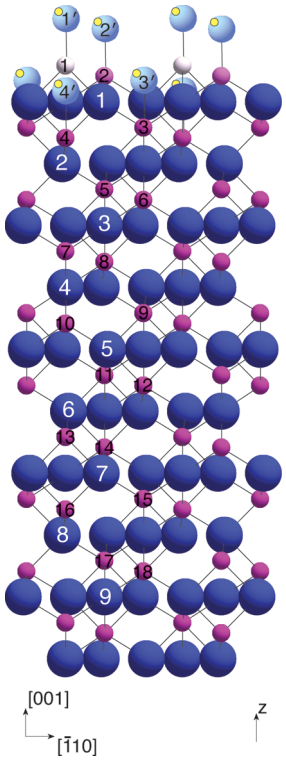

Figure 6. Ball and stick model (side view) of the surface termination of α-$Cr_2O_3(0001)$ employed for fitting the SXRD data acquired at $p(H_2O) \sim 30$ mbar (Cr_2O_3–H_2O_{30mbar}). Larger (smaller) spheres are oxygen (chromium) atoms; the smallest spheres are hydrogen atoms, which are employed to indicate location of adsorbed OH/H_2O. The oxygen atoms of adsorbed OH/H_2O species are labeled with 1′, 2′, 3′, and 4′. Numerical labeling of atoms is employed for identification purposes.

O(4′)) were constrained to have the same value during optimization.

DISCUSSION

Figure 7 summarizes the change in surface termination of α-$Cr_2O_3(0001)$ determined through analysis of the SXRD data acquired from Cr_2O_3–H_2O_{UHV} and Cr_2O_3–H_2O_{30mbar}. In the presence of ~30 mbar of H_2O, each under-coordinated surface Cr atom becomes decorated with a single atop OH/H_2O species. The lack of OH/H_2O on Cr_2O_3–H_2O_{UHV} is unexpected given that previous investigations of H_2O adsorption on α-$Cr_2O_3(0001)$ have revealed the presence of adsorbed OH at room temperature even in UHV;[3,4] H_2O exposures in these earlier studies were significantly lower than those employed in the present work. One possible explanation for this discrepancy is that the impinging X-ray beam could induce adsorbate desorption. Such a process would still occur at $p(H_2O) \sim 30$ mbar, but the OH/H_2O overlayer would be dynamically maintained due to the continuous flux of surface impinging H_2O molecules. Alternatively, it may be that under UHV conditions the surface coverage of OH/H_2O species is simply significantly lower than at 30 mbar (e.g., OH/H_2O may only be located at specific defect sites), and so the diffraction data are not sensitive to their presence. This possibility seems to contradict the previous studies,[3,4] which suggest that adsorption is not restricted to minority sites at room temperature in UHV. However, it should be noted that these studies were undertaken on thin films of α-$Cr_2O_3(0001)$, rather than a suitably oriented single crystal. It could very well be that this difference in substrate leads to variation in H_2O adsorption, i.e. thin films of α-$Cr_2O_3(0001)$ may display significant

Table 3. Optimized (x, y, z) Coordinates of Atoms Comprising the Cr_2O_3–H_2O_{30mbar} Surface Derived from Analysis of the SXRD Data Presented in Figure 5[a]

	(x, y, z) coordinates (Å)	
atom	bulk-terminated	optimized
$O_{0.08\pm0.01}(1')$	N/A	*3.31**, *1.65**, 25.10 ± 0.05
$O_{0.28\pm0.01}(2')$	N/A	*0.00**, *0.00**, 24.36 ± 0.02
$Cr_{0.08\pm0.01}(1)$	3.31, 1.65, 22.65	*3.31**, *1.65**, 22.79 ± 0.05
$Cr_{0.28\pm0.01}(2)$	0.00, 0.00, 22.27	*0.00**, *0.00**, 22.05 ± 0.02
$O_{0.30\pm0.01}(3')$	N/A	*1.65**, *3.31**, 22.83 ± 0.01
$O_{0.60\pm0.01}(4')$	N/A	*3.31**, *1.65**, 22.58 ± 0.01
$O_{0.40\pm0.03}(1)$	1.79, 1.65, 21.33	1.76 ± 0.02, 1.74 ± 0.03, 21.25 ± 0.05
$Cr_{0.70\pm0.01}(3)$	1.65, 3.31, 20.39	*1.65**, *3.31**, 20.52 ± 0.01
Cr(4)	3.31, 1.65, 20.00	*3.31**, *1.65**, 20.27 ± 0.01
O(2)	1.65, −0.14, 19.06	1.66 ± 0.01, −0.14 ± 0.02, 19.06 ± 0.02
Cr(5)	0.00, 0.00, 18.12	*0.00**, *0.00**, 18.22 ± 0.01
Cr(6)	1.65, 3.31, 17.74	*1.65**, *3.31**, 17.83 ± 0.01
O(3)	1.52, 1.52, 16.80	1.54 ± 0.02, 1.54 ± 0.01, 16.96 ± 0.02
Cr(7)	3.31, 1.65, 15.86	*3.31**, *1.65**, 15.99 ± 0.01
Cr(8)	0.00, 0.00, 15.47	*0.00**, *0.00**, 15.54 ± 0.01
O(4)	1.79, 0.14, 14.53	1.77 ± 0.02, 0.01 ± 0.01, 14.63 ± 0.02
Cr(9)	1.65, 3.31, 13.59	*1.65**, *3.31**, 13.74 ± 0.01
Cr(10)	3.31, 1.65, 13.21	*3.31**, *1.65**, 13.28 ± 0.01
O(5)	1.65, 1.79, 12.27	1.69 ± 0.01, 1.76 ± 0.02, 12.30 ± 0.02
Cr(11)	0.00, 0.00, 11.33	*0.00**, *0.00**, 11.39 ± 0.01
Cr(12)	1.65, 3.31, 10.94	*1.65**, *3.31**, 11.02 ± 0.01
O(6)	1.52, 0.00, 10.00	1.52*, 0.00*, 10.06 ± 0.01
Cr(13)	3.31, 1.65, 9.06	*3.31**, *1.65**, 9.12 ± 0.01
Cr(14)	0.00, 0.00, 8.68	*0.00**, *0.00**, 8.73 ± 0.01
O(7)	1.79, 1.65, 7.74	1.79*, 1.65*, 7.78 ± 0.01
Cr(15)	1.65, 3.31, 6.80	*1.65**, *3.31**, 6.85 ± 0.01
Cr(16)	3.31, 1.65, 6.41	*3.31**, *1.65**, 6.45 ± 0.01
O(8)	1.65, −0.14, 5.47	1.65*, −0.14*, 5.50 ± 0.01
Cr(17)	0.00, 0.00, 4.53	*0.00**, *0.00**, 4.57 ± 0.01
Cr(18)	1.65, 3.31, 4.15	*1.65**, *3.31**, 4.16 ± 0.01
O(9)	1.52, 1.52, 3.20	1.52*, 1.52*, 3.22 ± 0.03

[a]Fractional occupancy is indicated by a non-integer subscript in the "atom" column; the overall occupancy of oxygen atoms in the layer containing O(1) is 1.2 ± 0.09, as there are three symmetry equivalent oxygen atoms per (1 × 1) unit cell. Atomic coordinates for the bulk-terminated Cr–Cr–O_3-structure are also listed. Figure 6 provides a key to the identity of the atoms. An asterisk (∗) indicates that the parameter has been held constant during optimization. x and y coordinates not optimized due to symmetry constraints are italicized.

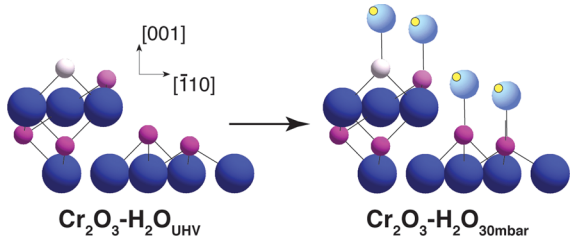

Figure 7. Cartoon of the variation in surface termination of α-$Cr_2O_3(0001)$ with water partial pressure, as determined through analysis of the SXRD data acquired from Cr_2O_3–H_2O_{UHV} and Cr_2O_3–H_2O_{30mbar}.

DOI: 10.1021/acs.jpcc.5b04607
J. Phys. Chem. C 2015, 119, 21426–21433

concentrations of sites active for dissociative adsorption of H_2O that are not present to any significant extent on the single crystal substrate. Finally, it is concluded in ref 4 that surface-bound OH is expected to slowly desorb from α-$Cr_2O_3(0001)$ at around room temperature. Such loss of OH, if it occurs, would likely result in SXRD data being acquired in UHV from a surface with a coverage of OH well below saturation. However, this desorption process is probably not the origin of the observed lack of adsorbed OH/H_2O on Cr_2O_3–H_2O_{UHV}. If it were, one might expect an OH/H_2O overlayer close to saturation coverage to be maintained on the surface at H_2O partial pressures well below 30 mbar, which is not reflected by the plot in Figure 2, i.e., would expect increase in diffracted signal to occur at lower $p(H_2O)$.

Concerning the structure determined at $p(H_2O) \sim 30$ mbar, it can be seen that it is inconsistent with the predictions emerging from the calculations of Costa et al.[6] They conclude that a (OH)–Cr–O_3– termination is energetically unfavorable, contradicting our experimental structure determination. It may be argued that this discrepancy is again due to the influence of the X-ray beam. However, in our opinion, that the X-ray beam would selectively desorb OH/H_2O species from each surface Cr leaving one remaining is doubtful. One more plausible reason for this difference, as stated in the Experimental Methods, is that the SXRD data have been acquired from a surface submerged beneath multiple monolayers of H_2O, due to the relative humidity being ~100%.[11] In contrast, Costa et al. do not explicitly include multiple layers of water in their modeling,[6] which may be the origin of the variation in interfacial structure. An alternative explanation for the divergence between the *ab initio* predictions and experiment is that the initial clean substrate termination used for the calculations is significantly different to that determined by diffraction. It could be that the more disordered surface found in the experiment hinders the formation of an extended network of OH/H_2O hydrogen bonding, which emerges from the first-principles modeling, resulting in Cr binding to multiple OH/H_2O species becoming energetically unfavorable. Another possible reason for the difference is that there is a significant energy barrier to the attachment of additional OH/H_2O to each Cr, and so cannot be realized with the substrate at room temperature. Further *ab initio* modeling, which more closely mimics both the experimentally determined α-$Cr_2O_3(0001)$ termination and the measurement environment, is required to test these hypotheses. For example, *ab initio* molecular dynamics could be employed to better simulate the submerged substrate.[16]

Regarding the precise nature of the adsorbed species at 30 mbar of H_2O, only the Cr–(OH/H_2O) interatomic distances (i.e., $Cr(1)$–$O(1')$, $Cr(2)$–$O(2')$, $Cr(3)$–$O(3')$, and $Cr(4)$–$O(4')$) provides any direct insight. As indicated above, a value of 2.09 Å, with an error bar ranging from ±0.01 Å for $Cr(3)$–$O(3')$ and $Cr(4)$–$O(4')$ to ±0.07 Å for $Cr(1)$–$O(1')$, has been obtained for this parameter; the spread in the magnitude of the errors is a result of the variation in fractional occupancies (lower occupancy leads to a larger error.). Costa et al. predict that the Cr–O bond length for a surface bound OH moiety should be 1.97 Å, increasing to 2.1 Å for adsorbed H_2O.[6] On this basis, one might propose that at 30 mbar of H_2O, $Cr_2O_3(0001)$ is decorated with adsorbed molecular H_2O rather than OH. However, this deduction must be regarded with caution due to the approach employed for fitting the diffraction data, i.e. to limit the number of parameters optimized, the possibility for each substrate atom to adopt more than one location was not incorporated, even where there were variations in local environment. For example, regarding the Cr_2O_3–H_2O_{30mbar} data, this approach results in employing only two atoms ($Cr(3)$ and $Cr(4)$) to describe the first subsurface double layer of Cr atoms, even though some are bound to $O(1)$ and others to $O(3')$ or $O(4')$ atoms. Given that this change in local coordination is likely to lead to somewhat different atomic coordinates, the Cr-(OH/H_2O) inter atomic distance (2.09 Å) is less well-defined than indicated above. Consequently, we conclude that it is not possible to uniquely identify the adsorbate (OH or H_2O) present on Cr_2O_3–H_2O_{30mbar} from the current SXRD data set. However, the weight of other evidence[3,4,6] suggests that dissociative adsorption is more likely, i.e. the adsorbate is OH.

Comparing the present results to those obtained for the interaction of H_2O with other (0001) surfaces of corundum-type metal oxides, of particular interest are near ambient pressure photoemission data from α-$Fe_2O_3(0001)$.[17] In that study, it was concluded that as the partial pressure of H_2O increases, the surface becomes increasingly decorated with surface OH, attaining a maximum coverage of ~1 monolayer at $\sim 10^{-4}$ mbar. Adsorbed H_2O is also observed, suggested to be located above the OH layer, i.e. a three layer $Fe_2O_3(0001)$/OH/H_2O interface is formed. One might also expect similar layering on α-$Cr_2O_3(0001)$ at 30 mbar of H_2O, but only a single OH/H_2O layer is evident from analysis of the SXRD data. However, it should be remembered that SXRD is sensitive to adsorbed layers displaying order both parallel and perpendicular to the surface plane of the substrate. Hence, the analysis presented here should not be interpreted as indicating that only a single layer of OH/H_2O is present on $Cr_2O_3(0001)$ at 30 mbar H_2O, but that only this layer is sufficiently ordered to be apparent in SXRD. Again, 30 mbar of H_2O is equivalent to ~100% relative humidity with the substrate at room temperature, and so the surface is expected to be submerged beneath multiple monolayers of H_2O.[11]

Another result worthy of mention is the local adsorption geometry of OH obtained from photoelectron diffraction (PhD) measurements in UHV performed following exposure of $V_2O_3(0001)$ to H_2O.[18] In contrast to the current study, no evidence for OH atop surface V atoms was found. Instead, only the surface oxygen atoms (equivalent to $O(1)$ in Figures 4 and 6) are hydroxylated through attachment of H, presumably derived from H_2O dissociation; the location of the dissociated OH fragment is not identified. This difference may be due to the initial $V_2O_3(0001)$ surface being terminated by vanadyl groups (V=O), rather than under-coordinated V atoms.[18]

Of further interest is a brief consideration of the previous SXRD study probing the surface structure α-$Cr_2O_3(0001)$ as a function of oxygen partial pressure.[7] It is pleasing to note that away from UHV ($p(H_2O) \sim 30$ mbar (current study), and $p(O_2) = 1 \times 10^{-2}$ mbar[7]) the optimum surface structures are not identical, i.e. data have not simply been acquired from similarly contaminated surfaces due to extrinsic components of the ambient environment. For both H_2O and O_2, adsorption occurs atop under-coordinated surface Cr atoms, but the Cr–O bond distance is significantly shorter in the presence of O_2 (1.57 ± 0.03 Å). This shorter Cr–O distance is consistent with the formation of surface chromyl (Cr=O) groups.[7] Furthermore, unlike H_2O/OH decorated α-$Cr_2O_3(0001)$, the chromyl terminated surface remains intact following reduction of the O_2 partial pressure.

DOI: 10.1021/acs.jpcc.5b04607
J. Phys. Chem. C 2015, 119, 21426–21433

CONCLUSIONS

To summarize, SXRD data have been acquired from α-Cr_2O_3(0001) as a function of H_2O partial pressure. In UHV, after exposure to ~2000 L of H_2O, the surface is terminated by a partially occupied double layer of chromium atoms; the lack of adsorbed OH/H_2O is concluded to be most likely a result of either adsorption only at defects, or X-ray induced desorption. This surface geometry is largely consistent with those determined in recent LEED-IV[15] and SXRD[7] studies of clean α-Cr_2O_3(0001) in UHV, although there are differences in the values of atomic coordinates and fractional layer occupancies. At ~ 30 mbar of H_2O, a single OH/H_2O species is bound atop each surface Cr. This result is not consistent with the *ab initio* calculations of Costa et al.,[6] which predict that surface termination evolves as a function of H_2O partial pressure at around room temperature as Cr−O_3−Cr− → $(OH)_2$−Cr−O_3− → $(H_2O(OH)_2)$−Cr−O_3−. One possible explanation for this discrepancy between theory and experiment is that the calculations do not explicitly take into account multiple layers of interfacial H_2O, which is the expected SXRD measurement environment, as the relative humidity is ~100%.

ASSOCIATED CONTENT

Supporting Information

The Supporting Information is available free of charge on the ACS Publications website at DOI: 10.1021/acs.jpcc.5b04607.

LEED and Auger data acquired from Cr_2O_3(0001) substrate (PDF)

AUTHOR INFORMATION

Corresponding Author

*(R.L). Telephone: +44 161 306 4824 Fax: +44 161 306 4865 Email: robert.lindsay@manchester.ac.uk.

Notes

The authors declare no competing financial interest.

[#]Deceased.

ACKNOWLEDGMENTS

M.H.M.A. acknowledges financial support from EPSRC through the Advanced Metallic Systems Centre for Doctoral Training (EP/G036950/1) and from BP. J.P.W.T. acknowledges financial support from Diamond Light Source and EPSRC. H.H. acknowledges financial support from the ESRF and EPSRC. X.T. thanks MICINN for financial support through Project MAT2012-38213-CO2-02. G.T. acknowledges support from the European Research Council Advanced Grant (ENERGYSURF), EU COST Action 1104, and the Royal Society.

REFERENCES

(1) Iverson, A.; Leffler, B. Shreir's Corrosion, Vol. 3, *Corrosion and Degradation of Engineering Materials*; Elsevier: Amsterdam, 2010.

(2) Maurice, V.; Marcus, P. *Tribocorrosion of Passive Films and Coatings*; Woodhead Publishing Limited: Cambridge, U.K., 2011.

(3) Henderson, M. A.; Chambers, S. A. HREELS, TPD and XPS Study of the Interaction of Water with the α-Cr_2O_3(0001) Surface. *Surf. Sci.* **2000**, *449*, 135−150.

(4) Maurice, V.; Cadot, S.; Marcus, P. Hydroxylation of Ultra-Thin Films of α-Cr_2O_3(0001) Formed on Cr(110). *Surf. Sci.* **2001**, *471*, 43−58.

(5) Petrosyan, S. A.; Rigos, A. A.; Arias, T. A. Joint Density-Functional Theory: Ab Initio Study of Cr_2O_3 Surface Chemistry in Solution. *J. Phys. Chem. B* **2005**, *109*, 15436−15444.

(6) Costa, D.; Sharkas, K.; Islam, M. M.; Marcus, P. *Ab initio* Study of the Chemical States of Water on Cr_2O_3(0001): From Isolated Molecule to Saturation Coverage. *Surf. Sci.* **2009**, *603*, 2484−2493.

(7) Bikondoa, O.; Moritz, W.; Torrelles, X.; Kim, H. J.; Thornton, G.; Lindsay, R. Impact of Ambient Oxygen on the Surface Structure of α-Cr_2O_3(0001). *Phys. Rev. B: Condens. Matter Mater. Phys.* **2010**, *81*, 205439.

(8) Woodruff, D. P. Quantitative Structural Studies of Corundum and Rocksalt Oxide Surfaces. *Chem. Rev.* **2013**, *113*, 3863−3886.

(9) Kuhlenbeck, H.; Shaikhutdinov, S.; Freund, H. J. Well-Ordered Transition Metal Oxide Layers in Model Catalysis − A Series of Case Studies. *Chem. Rev.* **2013**, *113*, 3986−4034.

(10) Kaspar, T. C.; Chamberlin, S. E.; Chambers, S. A. Surface Structure of α-Cr_2O_3(0001) After Activated Oxygen Exposure. *Surf. Sci.* **2013**, *618*, 159−166.

(11) Ketteler, G.; Yamamoto, S.; Bluhm, H.; Andersson, K.; Starr, D. E.; Ogletree, D. F.; Ogasawara, H.; Nilsson, A.; Salmeron, M. The Nature of Water Nucleation Sites on TiO_2(110) Surfaces Revealed by Ambient Pressure X-ray Photoelectron Spectroscopy. *J. Phys. Chem. C* **2007**, *111*, 8278−8282.

(12) Vlieg, E. A. (2 + 3)-Type Surface Diffractometer: Mergence of the z-Axis and (2 + 2)-Type Geometries. *J. Appl. Crystallogr.* **1998**, *31*, 198−203.

(13) Vlieg, E. ROD: a Program for Surface X-ray Crystallography. *J. Appl. Crystallogr.* **2000**, *33*, 401−405.

(14) Fiedenhans'l, R. Surface Structure Determination by X-ray Diffraction. *Surf. Sci. Rep.* **1989**, *10*, 105−188.

(15) Lübbe, M.; Moritz, W. A LEED Analysis of Clean Substrates of α-Fe_2O_3(0001) and α-Cr_2O_3(0001) Bulk Single Crystals. *J. Phys.: Condens. Matter* **2009**, *21*, 134010.

(16) Carrasco, J.; Hodgson, A.; Michaelides, A. A Molecular Perspective of Water at Metal Interfaces. *Nat. Mater.* **2012**, *11*, 667−674.

(17) Yamamoto, S.; Kendelewicz, T.; Newberg, J. T.; Ketteler, G.; Starr, D. E.; Mysak, E. R.; Andersson, K. J.; Ogasawara, H.; Bluhm, H.; Salmeron, M.; et al. Water Adsorption on α-Fe_2O_3(0001) at near Ambient Conditions. *J. Phys. Chem. C* **2010**, *114*, 2256−2266.

(18) Kröger, E. A.; Sayago, D. I.; Allegretti, F.; Knight, M. J.; Polcik, M.; Unterberger, W.; Lerotholi, T. J.; Hogan, K. A.; Lamont, C. L. A.; Cavalleri, M.; et al. The Local Structure of OH Species on the V_2O_3(0001) Surface: A Scanned-Energy Mode Photoelectron Diffraction Study. *Surf. Sci.* **2008**, *602*, 1267−1279.

DOI: 10.1021/acs.jpcc.5b04607
J. Phys. Chem. C 2015, 119, 21426−21433